of photophobia [MacLeod, 1909]. Martino et al. [1992] reported a male patient with IFAP syndrome presented with short stature, intellectual disability, seizures, hypohidrosis, enamel dysplasia, congenital aganglionic megacolon, inguinal hernia, vertebral and renal anomalies, and the classic symptom triad of IFAP syndrome. This report broadened the clinical features of IFAP syndrome. It should be noted that the clinical symptoms of this patient are quite similar to those of BRESHECK syndrome, with the exception of cleft palate, cryptorchidism, and photophobia (Patient 5; Table I). The gene mutated in patients with IFAP syndrome, *MBTPS2* (GenBank reference sequence NM_015884), was identified from a variety of clinical features of IFAP syndrome, including the triad and neonatal death [Oeffner et al., 2009]. Thus, the mode of inheritance and several clinical features are common to both BRESEK/BRESHECK and IFAP syndromes. These findings prompted us to perform mutation analysis of *MBTPS2* in the present patient, resulting in the identification of a missense mutation.

MATERIALS AND METHODS

Patients

Written informed consent was obtained from the parents of the patient. Experiments were conducted after approval of the institutional review board of the Institute for Developmental Research, Aichi Human Service Center. The patient (II-1; Fig. 3) was born to a 31-year-old mother (I-2) and a 31-year-old father (I-1), both healthy Japanese individuals without consanguinity. His mother miscarried her first child at 5 weeks. The pregnancy of the patient reported here was complicated with mild oligohydramnios, and he was delivered by caesarean because of a breech position at 38 weeks of gestation. His birth weight was 1,996 g (−2.6 SD), and he measured 44 cm (−2.6 SD) in length with an occipitofrontal circumference of 32.5 cm (−0.5 SD). Apgar scores at 1 and 5 min were four and eight, respectively. The patient exhibited generalized alopecia and lacked eyelashes, scalp hair, and eyebrows (Fig. 1A). The skin on the entire body was erythematous with

TABLE I. Clinical Features of BRESEK/BRESHECK and IFAP Syndromes and *MBTPS2* Mutation

	BRESEK/BRESHECK syndrome				IFAP syndrome		
Patient	1	2	3	4	5	6	7
Clinical features							
Gender	M	M	M	M	M	M	M
Gestational age (weeks)	32	40	ND	38	30	ND	ND
Birth weight (g)	990	2,230	ND	1,996	2,040	ND	ND
Intrauterine growth retardation	+	+	ND	+	−	ND	ND
Major features							
Follicular ichthyosis	−	−	ND	−	+	+	+
Atrichia	+	+	+	+	+	+	+
Photophobia	−	−	−	+	+	+	+
Brain malformation	+	+	+	+	+	−	+
Mental and growth retardation	+	+	+	+	+	+	+
Skeletal (Vertebrate) anomalies	+	+	+	+	+	+	+
Hirschsprung disease	−	+	+	+	+	+	+
Eye malformation or	+	+	+	−	+	−	−
Large ears	+	+	+	+	+	−	−
Cleft lip/palate or	−	+	−	−	−	+	−
Cryptorchidism	+	+	−	+	−	−	−
Kidney malformation	+	+	−	+	+	+	+
Other features							
Microcephaly	+	+	+	+	+	−	+
Seizures	−	+	+	+	+	−	+
Deafness	−	+	−	+	−	−	−
Hand anomalies	+	+	+	−	+	+	+
Cardiac anomalies	−	−	+	−	−	−	+
Inguinal hernia	−	−	−	−	+	+	+
Trachea anomalies	−	−	−	+	−	−	−
Regression	−	−	−	+	−	−	−
Age	6 h d	7 y	1.5 y	8 y	3 y	9 m d	14 m d
MBTPS2 mutation	NP	NP	NP	R429H	NP	R429H	R429H

+, present; −, not present; M, male; ND, not described; NP, not performed; h, hour; d, dead; m, month; y, year; R429H, Arg429His; BRESEK/BRESHECK syndrome, (Patients 1-4); IFAP syndrome, (Patients 5–7); Patients: 1, Reish et al. [1997] patient 1; 2, Reish et al. [1997] patient 2; 3, Tumialán and Mapstone [2006]; 4, present case; 5, Martino et al. [1992]; 6, Oeffner et al. [2009] 3-III:3; 7, Oeffner et al. [2009] 3-III:4.
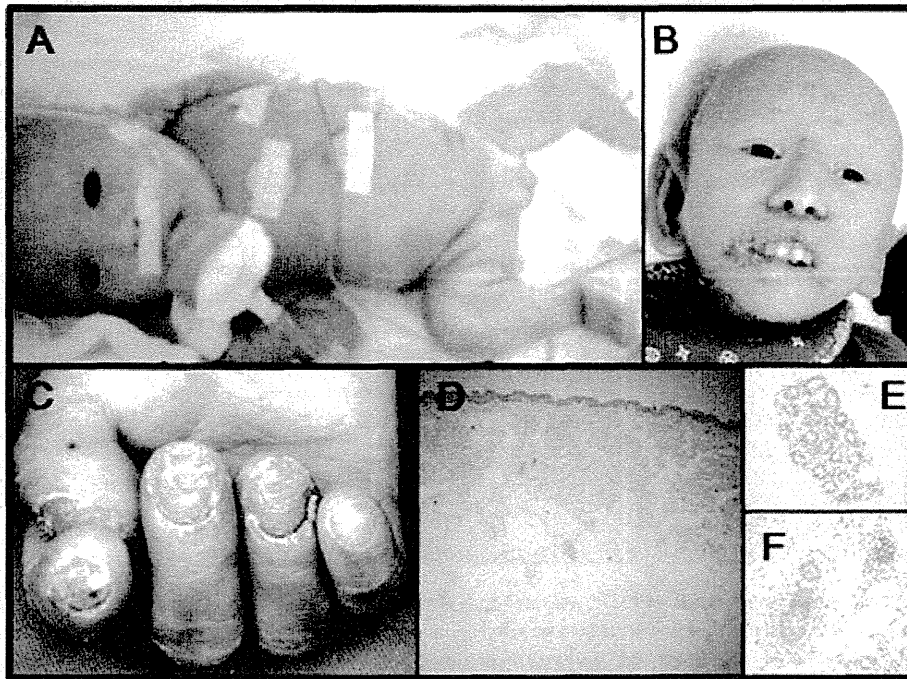
FIG. 1. Clinical appearance and dermatological findings of the patient. A: Lateral view of the patient at birth. Note the generalized alopecia with an absence of scalp hair, eyebrows, and eyelashes. The skin was dry and scaly, and an itchy erythema was observed over the entire body. B: Frontal view of the patient at 4 years of age. Note the characteristic facial appearance with long, malformed ears, a relatively high nasal bridge, and a wide nasal base. C: The patient had normal-sized but deformed and thickened nails. D–F: Histologic examination of the abdominal skin at the age of 15 months showed a reduced number of hair follicles (D), normal eccrine glands (E), and hypoplastic hair follicles (F).

continuous desquamation (Fig. 1A). He had malformed large ears, an inferiorly curved penis, and a bifid scrotum. The testicles were not palpable. He experienced persistent constipation, and total colonic Hirschsprung disease was confirmed through barium enema (Fig. 2E) and rectal biopsy at 2 months. A bone survey performed using three-dimensional (3D) computed tomography (CT) showed abnormal imbalanced hemivertebrae in the two lowest thoracic vertebral bodies (Fig. 2C). The patient's right kidney was smaller than normal. Brain magnetic resonance imaging (MRI) at 3 years of age demonstrated decreased volumes of the frontal and parietal lobes and thinning of the corpus callosum with dilatation of the ventricles (Fig. 2A,B). There were no abnormalities of the eyes or optic nerves. We concluded that the patient had BRESHECK syndrome. The patient had seizures at 5 months of age with an apneic episode and cyanosis. Electro-encephalographic (EEG) analysis showed abnormal patterns of sharp waves in the posterior lobe. The seizures were almost completely controlled with phenobarbital. The patient was allergic to milk. At 7 months, tracheal endoscopy revealed subglottic tracheal stenosis and abnormal segmentation of the left lung. A chest CT performed at 3 years of age showed a congenital cystic adenomatoid malformation (CCAM) in the right upper lobe (Fig. 2D). Auditory brain stem responses showed bilateral 80 dB hearing loss at 8 months of age.

The patient exhibited delayed psychomotor development during his infancy. He could drink from a bottle at the age of 3 months and could sit up unsupported at 15 months. Abdominal skin biopsy at 15 months revealed reduced number of hair follicles (Fig. 1D). The eccrine glands were normal (Fig. 1E), and most of his hair follicles appeared to be hypoplastic (Fig. 1F). These findings were similar to ichthyosiform erythroderma. Photophobia was noted when the patient left the hospital and first went outside at 18 months of age. At 2 years and 6 months of age, he had a series of epileptic episodes. He experienced a maximum of 100 seizures per day, and EEG analysis showed continual abnormal spikes in the posterior lobe. The seizures were controlled with clonazepam therapy. At 2 years and 9 months of age, he could stand with support and displayed social smiles when interacting with other people. However, the patient developed psychomotor regression at the age of 3 years. He exhibited a progressive loss of emotional response to others, developed hypotonia, and could not stand or sit alone. At 4 years of age, he became bedridden and showed almost no response to people. He had highly desquamated skin, similar to that seen in ichthyosis (Fig. 1B), and easily developed erythema on the skin of the entire body. The patient had deformed and thickened nails (Fig. 1C). He had persistent corneal erosions, but ophthalmoscopy could not be performed at the age of 4 years because of corneal opacification.
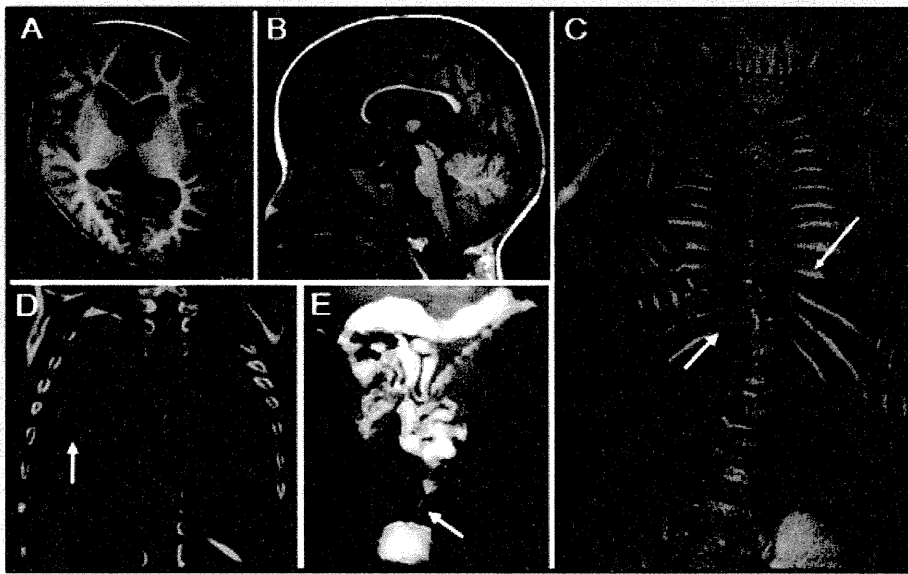
FIG. 2. CT and MRI findings of the patient. A,B: Brain MRI (T1-weighted image) at 3 years of age showed decreased volume of the cortex in the frontal and parietal lobes, the presence of a subdural cyst in the corpora quadrigemina, and dilatation of the lateral and fourth ventricle. C: A bone survey performed using 3D CT showed abnormal segmentation of the ninth rib and an imbalanced hemivertebrae in the two lowest thoracic vertebral bodies (shown with arrows). D: CT of the chest showed CCAM (indicated by the arrow) in the right upper lobe. E: Barium enema showed a reduced caliber rectum (indicated by the arrow), suggesting that the patient had Hirschsprung disease.

Chromosomal and Molecular Genetic Studies

Genomic DNA isolated from the patient's peripheral white cells by phenol/chloroform extraction was used for *MBTPS2* mutation analysis. PCR-amplified DNA fragments were isolated using the QIAEX II Gel Extraction Kit (Qiagen, Valencia, CA) and purified using polyethylene glycol 6000 precipitation. PCR products were sequenced with the Big Dye Terminator Cycle Sequencing Kit V1.1 and analyzed with the ABI PRISM 310 Genetic Analyzer (Life Technologies, Carlsbad, CA). We also performed G-banded chromosome analysis at a resolution of 400–550 bands, genome-wide subtelomere fluorescence in situ hybridization (FISH) analysis, and array comparative genomic hybridization (array CGH) using Whole Human Genome Oligo Microarray Kits 244K (Agilent Technologies Inc., Palo Alto, CA) to identify genomic abnormalities.

RESULTS

G-banded chromosome analysis and genome-wide subtelomere FISH analyses did not show chromosomal rearrangements in the patient. Array CGH analysis did not show copy number changes in the patient's genome with the exception of known copy-number variations (CNVs). Since some patients with IFAP syndrome have been reported to present with several clinical features of BRESEK/ BRESHECK syndrome, including severe intellectual disability, vertebral and renal anomalies, and Hirschsprung disease, we conducted a comprehensive sequencing analysis of all exons and intron–exon boundaries of *MBTPS2*. This analysis identified a

missense mutation (c.1286G>A, [p.Arg429His]) in exon 10, which was previously reported for IFAP syndrome (Fig. 3). The mutation was also found in one allele of the mother (I-2), indicating that the mutation was of maternal origin and that the mother was a heterozygous carrier (Fig. 3).

DISCUSSION

In this report, we describe the fourth male patient with BRESHECK syndrome in whom we identified a missense mutation (c.1286G>A, [p.Arg429His]) in *MBTPS2*, which is the causal gene for IFAP syndrome. *MBTPS2* encodes a membrane-embedded zinc metalloprotease, termed site-2 protease (S2P). S2P cleaves and activates cytosolic fragments of sterol regulatory element binding proteins (SREBP1 and SREBP2) and a family of bZIP membrane-bound transcription factors of endoplasmic reticulum (ER) stress sensors (ATF6, OASIS), after a first luminal proteolytic cut by site-1 protease (S1P) within Golgi membranes [Sakai et al., 1996; Ye et al., 2000; Kondo et al., 2005; Asada et al., 2011]. The SREBPs control the expression of many genes involved in the biosynthesis and uptake of cholesterol, whereas ATF6 and OASIS induce many genes that clean up accumulated unfolded proteins in the ER. Dysregulated SREBP activation, impaired lipid metabolism, and accumulation of unfolded proteins in the ER caused by *MBTPS2* mutations could lead to disturbed differentiation of epidermal structures, resulting in the symptom triad of IFAP syndrome [Cursiefen et al., 1999; Traboulsi et al., 2004; Elias et al., 2008]. Oeffner et al. [2009] first identified five missense mutations in *MBTPS2* in patients with IFAP
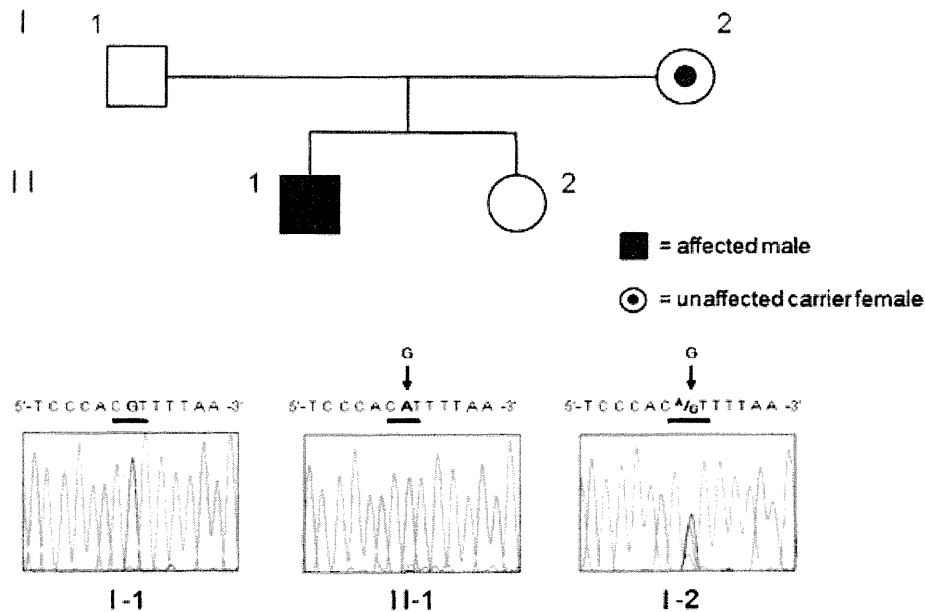
FIG. 3. Identification of a disease mutation. The sequence analyses of the patient (II-1) showed a c.1286G>A variant in exon 10 of *MBTPS2*, which predicts p.Arg429His, as indicated by the arrow (middle panel). The mother (I-2) was heterozygous for the mutation ($C^A/_GT$) (right panel).

syndrome. Transfection studies using wild type and mutant *MBTPS2* expression constructs demonstrated that the five *MBTPS2* mutations did not affect S2P protein amount and localization in the ER. However, enzyme activities, as measured by sterol responsiveness, were decreased in S2P-deficient M19 cells when the mutant *MBTPS2* was transiently expressed. Interfamilial phenotypic differences between male IFAP patients and the properties of mutants in functional assays predict a genotype–phenotype correlation, ranging from mild forms of the triad with relatively high enzyme activity (~80%) to severe manifestations of intellectual disability, various developmental defects, and early death with low enzyme activity (~15%). The identified p.Arg429His mutation in the patient reported here is one of the five missense mutations with the lowest enzyme activity. It was previously reported that all four patients harboring the p.Arg429His mutation died within 14 months of birth. The five mutations were not located in the HEIGH motif (amino acids [aa] 171–175) or in the $LD_{467}G$ sequence, both of which are regions important for coordinating the zinc atom at the enzymatic active site for protease activity in the Golgi membrane [Zelenski et al., 1999]. However, among the five mutations, the p.Arg429His mutation is located closest to the intramembranous domain, and it strongly reduced the enzymatic activity and caused a severe phenotype. This finding suggests that mutations in the HEIGH motif or in the $LD_{467}G$ sequence are fatal because they lead to a null function of the S2P. Although the detailed skin findings of the four patients with the p.Arg429His mutation have not been reported, it should be noted that one of the four patients (3-III:4) with the p.Arg429His mutation had brain anomaly, seizures, psychomotor retardation, vertebrae anomaly, Hirschsprung disease, absence of a kidney, atrial septum defect, and inguinal

hernia, in addition to the symptom triad of IFAP syndrome [Oeffner et al., 2009]. These symptoms overlap with the majority of symptoms observed in BRESHECK syndrome (BRESHK; six of eight symptoms observed in BRESHECK) (Table I), and the present patient has BRESHECK syndrome. Collectively, these observations suggest that the most severe form of the syndrome caused by the p.Arg429His mutation in *MBTPS2* shows features quite similar or identical to those of BRESEK/BRESHECK syndrome.

There are two major differences in the definitions of IFAP syndrome and BRESEK/BRESHECK syndrome. Ichthyosis follicularis, one of the triad symptoms of IFAP syndrome, is a clinical condition of the skin. However, several studies on IFAP syndrome have reported various skin eruptions such as psoriasis-like and ichthyosis-like eruptions [Martino et al., 1992; Sato-Matsumura et al., 2000]. In contrast, patients with BRESEK/BRESHECK syndrome showed severe lamellar desquamation with diffuse scaling [Reish et al., 1997], similar to that observed in the present patient. This could be because of the difference in features of the skin, namely, ichthyosiform erythroderma-like appearance versus ichthyosis follicularis, in patients with the most severe forms of *MBTPS2* mutation and patients with IFAP syndrome who were described earlier, respectively.

The second difference is that photophobia was not described in the reported three male patients with BRESEK/BRESHECK syndrome [Reish et al., 1997; Tumialán and Mapstone, 2006]. In the present patient, photophobia became evident after he was diagnosed with BRESHECK syndrome. Photophobia is a symptom of epithelial disturbances of the cornea, such as ulceration and vascularization, which result in corneal scarring [Traboulsi et al., 2004]. In the most severe cases of *MBTPS2* mutation, such as

patients with severe intellectual disability who are bedridden and die early, it is likely that the patients were treated in the hospital without being exposed to sunlight. Therefore, it would be difficult to observe photophobia as a main symptom in those cases. Moreover, two previously described patients with BRESEK/BRESHECK syndrome had initial maldevelopment of one eye or small optic nerves. In these patients, photophobia may not have been obvious because of malformations of the eyes and optic nerves [Reish et al., 1997]. In our study, the patient showed clinical features of BRESHECK syndrome and photophobia with *MBTPS2* mutation, indicating that the clinical features of the present patient are extremely broad compared to the features of IFAP syndrome caused by *MBTPS2* mutation that have been previously reported [MacLeod, 1909].

Recently, a missense mutation (c.1523A>G, [p.Asn508Ser]) in *MBTPS2* was identified from 26 cases of three independent families with keratosis follicularis spinulosa decalvans (KFSD; OMIM# 308800), which is characterized by the development of hyperkeratotic follicular papules on the scalp followed by progressive alopecia of the scalp, eyelashes, and eyebrows in addition to childhood photophobia and corneal dystrophy [Aten et al., 2010]. A significant association was found between KFSD and the p.Asn508Ser mutation. The specific localization of alopecia to the scalp, eyelashes, and eyebrows and the limited childhood photophobia of KFSD indicate that KFSD has a relatively mild phenotype. The authors postulate that IFAP syndrome and KFSD are within the spectrum of one genetic disorder with a partially overlapping phenotype and propose that a new name should be chosen for KFSD/IFAP syndrome with an *MBTPS2* mutation. In contrast, the BRESHECK syndrome observed in the present patient has a severe phenotype caused by the p.Arg429His mutation. The present patient and the two patients (3-III:3 and 3-III:4) with the p.Arg429His mutation displayed broader clinical features, including eight features (BRESHECK) and six features (RESHCK and BRESHK) of BRESEK/BRESHECK syndrome, respectively (patients 4, 6, and 7; Table I) [Oeffner et al., 2009]. There is a debate regarding whether the two patients harboring six features were correctly diagnosed with BRESEK/BRESHECK syndrome since the patients did not have "BRESEK" but rather a combination of six other clinical features. To better understand and clearly distinguish the clinical features of the present patient from those of the reported patients with *MBTPS2* mutations, we propose the nomenclature of "BRESHECK/IFAP syndrome" for the present patient because he has clinical features of BRESHECK syndrome. We also suggest that the BRESHECK/IFAP syndrome be used for a broader definition that would include patients harboring most features of BRESHECK syndrome, including the previously reported two patients (3-III:3 and 3-III:4) with p.Arg429His mutation in *MBTPS2* [Oeffner et al., 2009]. Data from further genetic and clinical studies on more patients are required to determine which genes or *MBTPS2* mutations are associated with BRESEK/BRESHECK or BRESHECK/IFAP syndrome, respectively.

REFERENCES

Aten E, Brasz LC, Bornholdt D, Hooijkaas IB, Porteous ME, Sybert VP, Vermeer MH, Vossen RH, van der Wielen MJ, Bakker E, Breuning MH, Grzeschik KH, Oosterwijk JC, den Dunnen JT. 2010. Keratosis follicularis spinulosa decalvans is caused by mutations in MBTPS2. Hum Mutat 31:1125–1133.

Asada R, Kanemoto S, Kondo S, Saito A, Imaizumi K. 2011. The signalling from endoplasmic reticulum-resident bZIP transcription factors involved in diverse cellular physiology. J Biochem 149:507–518.

Cursiefen C, Schlötzer-Schrehardt U, Holbach LM, Pfeiffer RA, Naumann GOH. 1999. Ocular findings in ichthyosis follicularis, atrichia, and photophobia syndrome. Arch Ophthalmol 117:681–684.

Elias PM, Williams ML, Holleran WM, Jiang YJ, Schmuth M. 2008. Pathogenesis of permeability barrier abnormalities in the ichthyoses: Inherited disorders of lipid metabolism. J Lipid Res 49:697–714.

Kondo S, Murakami T, Tatsumi K, Ogata M, Kanemoto S, Otori K, Iseki K, Wanaka A, Imaizumi K. 2005. OASIS, a CREB/ATF-family member, modulates UPR signalling in astrocytes. Nat Cell Biol 7:186–194.

MacLeod JMH. 1909. Three cases of 'ichthyosis follicularis' associated with baldness. Br J Dermatol 21:165–189.

Martino F, D'Eufemia P, Pergola MS, Finocchiaro R, Celli M, Giampà G, Frontali M, Giardini O. 1992. Child with manifestations of dermotrichic syndrome and ichthyosis follicularis alopecia photophobia (IFAP) syndrome. Am J Med Genet 44:233–236.

Oeffner F, Fischer G, Happle R, König A, Betz RC, Bornholdt D, Neidel U, Boente Mdel C, Redler S, Romero-Gomez J, Salhi A, Vera-Casaño A, Weirich C, Grzeschik KH. 2009. IFAP syndrome is caused by deficiency in MBTPS2, an intramembrane zinc metalloprotease essential for cholesterol homeostasis and ER stress response. Am J Hum Genet 84:459–467.

Reish O, Gorlin RJ, Hordinsky M, Rest EB, Burke B, Berry SA. 1997. Brain anomalies, retardation of mentality and growth, ectodermal dysplasia, skeletal malformations, Hirschsprung disease, ear deformity and deafness, eye hypoplasia, cleft palate, cryptorchidism, and kidney dysplasia/hypoplasia (BRESEK/BRESHECK): New X-linked syndrome? Am J Med Genet 68:386–390.

Sakai J, Duncan EA, Rawson RB, Hua X, Brown MS, Goldstein JL. 1996. Sterol-regulated release of SREBP-2 from cell membranes requires two sequential cleavages, one within a transmembrane segment. Cell 85:1037–1046.

Sato-Matsumura KC, Matsumura T, Kumakiri M, Hosokawa K, Nakamura H, Kobayashi H, Ohkawara A. 2000. Ichthyosis follicularis with alopecia and photophobia in a mother and daughter. Br J Dermatol 142:157–162.

Traboulsi E, Waked N, Mégarbané H, Mégarbané A. 2004. Ocular findings in ichthyosis follicularis–alopecia–photophobia (IFAP) syndrome. Ophthal Genet 25:153–156.

Tumialán LM, Mapstone TB. 2006. A rare cause of benign ventriculomegaly with associated syringomyelia: BRESEK/BRESHECK syndrome. Case illustration. J Neurosurg 105:155.

Ye J, Rawson RB, Komuro R, Chen X, Davé UP, Prywes R, Brown MS, Goldstein JL. 2000. ER stress induces cleavage of membrane-bound ATF6 by the same proteases that process SREBPs. Mol Cell 6:1355–1364.

Zelenski NG, Rawson RB, Brown MS, Goldstein JL. 1999. Membrane topology of S2P, a protein required for intramembranous cleavage of sterol regulatory element-binding proteins. J Biol Chem 274:21973–21980.

ORIGINAL INVESTIGATION

Novel intragenic duplications and mutations of *CASK* in patients with mental retardation and microcephaly with pontine and cerebellar hypoplasia (MICPCH)

Shin Hayashi · Nobuhiko Okamoto · Yasutsugu Chinen · Jun-ichi Takanashi ·
Yoshio Makita · Akira Hata · Issei Imoto · Johji Inazawa

Abstract The *CASK* gene encoding a member of the membrane-associated guanylate kinase protein family is highly expressed in the mammalian nervous system of both adults and fetuses, playing several roles in neural development and synaptic function. Recently, *CASK* aberrations caused by both mutations and deletions have been reported to cause severe mental retardation (MR), microcephaly and disproportionate pontine and cerebellar hypoplasia (MIC-PCH) in females. Here, mutations and copy numbers of *CASK* were examined in ten females with MR and MIC-PCH, and the following changes were detected: nonsense mutations in three cases, a 2-bp deletion in one case, mutations at exon–intron junctions in two cases, heterozygous deletions encompassing *CASK* in two cases and interstitial duplications in two cases. Except for the heterozygous deletions, each change including the intragenic duplications potentially caused an aberrant transcript, resulting in *CASK* null mutations. The results provide novel mutations and copy number aberrations of *CASK*, causing MR with MIC-PCH, and also demonstrate the similarity of the phenotypes of MR with MICPCH regardless of the *CASK* mutation.

Introduction

The *CASK* gene (OMIM: *300172) encoding a member of the membrane-associated guanylate kinase (MAGUK) protein family is highly expressed in the mammalian ner-

S. Hayashi · I. Imoto · J. Inazawa (✉)
Department of Molecular Cytogenetics, Medical Research
Institute and School of Biomedical Science, Tokyo Medical and
Dental University, 1-5-45 Yushima, Bunkyo-ku,
Tokyo 113-8510, Japan
e-mail: johinaz.cgen@mri.tmd.ac.jp

S. Hayashi
Hard Tissue Genome Research Center,
Tokyo Medical and Dental University, Tokyo, Japan

N. Okamoto
Department of Planning and Research, Osaka Medical Center and
Research Institute for Maternal and Child Health, Osaka, Japan

Y. Chinen
Department of Pediatrics, University of the Ryukyu School
of Medicine, Okinawa, Japan

J. Takanashi
Department of Pediatrics, Kameda Medical Center, Chiba, Japan

Y. Makita
Education Center, Asahikawa Medical College, Asahikawa, Japan

A. Hata
Department of Public Health, Chiba University Graduate School
of Medicine, Chiba, Japan

I. Imoto
Department of Human Genetics and Public Health Graduate
School of Medical Science, The University of Tokushima,
Tokushima, Japan

J. Inazawa
Global Center of Excellence (GCOE) Program for 'International
Research Center for Molecular Science in Tooth and Bone
Diseases', Tokyo Medical and Dental University,
Tokyo, Japan

🌱 Springer

vous system of both adults and fetuses (Stevenson et al. 2000), and plays several roles in neural development and synaptic function (Hsueh 2006). Recently, we have reported the possible involvement of the decrease of intact *CASK* expression induced by a microdeletion at Xp11.4 in the pathogenesis of mental retardation (MR) and microcephaly (Hayashi et al. 2008). Concurrently, Najm et al. (2008) reported that mutations of *CASK* caused severe MR, microcephaly, and disproportionate pontine and cerebellar hypoplasia (MICPCH, OMIM: #300749). To examine the involvement of point mutations and/or copy number variations (CNVs) of *CASK* in patients with MR and MICPCH, we performed DNA sequencing and molecular cytogenetic analyses including array-based comparative genomic hybridization (aCGH) in ten patients showing such phenotypes. Pathogenic alterations of *CASK* were detected in all ten cases, and each change including intragenic duplications caused a truncation of the gene.

Subjects and methods

Subjects

From three hospitals in Japan, we recruited ten Japanese females (patients 1–10) suspected of having *CASK* mutations based on phenotypic criteria: female, MR and MICPCH. All patients were examined and evaluated by clinical dysmorphologists in each hospital. Their clinical features are shown in Table 1.

Briefly, their ages at the last follow-up ranged from 11 months to 14 years. All were born by normal full-term deliveries. At birth, patients 1, 2, 3, 5 and 7 revealed obvious signs of microcephaly (<-2.0 SD) and at present all the patients show severe microcephaly; their development has been markedly retarded. Only patients 5 and 6 can walk, and only patient 9 can speak any words at all. Patients 1, 2, 7, 9 and 10 show muscular hypotonia. Magnetic resonance imaging (MRI) of the brain demonstrated similar aberrations; all patients revealed hypoplasia of the cerebellum, mesencephalon and pons (Fig. 1; Table 1). Conventional karyotyping of peripheral blood lymphocytes with approximately 400–550 bands revealed a normal female karyotype, 46,XX, in each patient.

All samples were obtained with prior written informed consent from the parents and approval by the local ethics committee and all the institutions involved in this project. A lymphoblastoid cell line (LCL) was established by infecting lymphocytes of the patients and patients' parents with Epstein–Barr virus, as described previously (Saito-Ohara et al. 2002).

Mutation analysis

Mutations within all coding sequences of *CASK* were analyzed by exon amplification and direct sequencing using primer combinations designed for genomic sequences around each exon (Najm et al. 2008). Any base changes detected in samples were confirmed by sequencing each product in both directions.

aCGH analysis

For patients in whom no mutation of *CASK* was detected, we performed aCGH to estimate the genomic copy number variant (CNV) around *CASK*. We employed an in-house bacterial artificial chromosome (BAC)-based array, the 'MCG X-tiling array' (X-Array) (Inazawa et al. 2004), which contains 1001 BAC/PACs throughout the X-chromosome other than pseudoautosomal regions for aCGH analysis (Hayashi et al. 2007). Hybridization was performed as described elsewhere (Hayashi et al. 2007). For two patients, we also applied an oligonucleotide array (Agilent Human Genome CGH Microarray 244K; Agilent Technologies, Santa Clara, CA, USA) to determine the boundaries of the CNVs identified with the X-Array. DNA labeling, hybridization and washing of the arrays were performed according to the directions provided by the manufacturer. The hybridized arrays were scanned using an Agilent scanner (G2565BA), and the CGH Analytics program version 3.4.40 (Agilent Technologies) was used to analyze CNVs after data extraction, filtering and normalization by Feature Extraction software (Agilent Technologies).

Fluorescence in situ hybridization (FISH)

FISH was performed as described elsewhere (Hayashi et al. 2005) using BAC clones located around the region of interest to confirm all the detected CNVs.

Genomic PCR and reverse transcription-PCR

Genomic PCR was performed on genomic DNA of the ten patients and an unaffected female as a control. Reverse transcription-PCR (RT-PCR) was performed on cDNA extracted from LCLs of patients 5, 6, 9 and 10 and an unaffected female as a control. The sequences of the primer combinations are provided in Supplementary Table 1.

Real-time quantitative PCR

To determine the boundaries of the duplications more precisely, real-time quantitative PCR (qPCR) was performed

Table 1 Clinical features and analysis of *CASK*

Patient	1	2	3	4	5	6	7	8	9	10
Gender	F	F	F	F	F	F	F	F	F	F
Age at last follow-up	2 years, 8 months	2 years, 0 month	2 years, 8 months	11 months	7 years, 9 months	14 years	1 years, 9 months	2 years, 0 months	12 years	7 years, 2 months
Gestational age (weeks)	41	41	40	41	40	41	36	41	41	41
Height at birth (SD)	NA	0.2	−2.6	−0.8	−3.8	−0.8	−2.2	−0.9	−2.0	0.2
Weight at birth (SD)	−1.9	−0.1	−1.6	−0.7	−2.2	−0.3	−2.9	−1.9	−1.1	0.4
OFC at birth (SD)	−3.2	−2.3	−2.8	−0.8	−3.4	−0.4	−4.3	−1.3	−1.9	−1.5
Height at last follow-up (SD)	−1.5	−2.7	−1.9	−1.7	−3.7	−4.9	−0.9	−3.0	−3.5	−3.0
Weight at last follow-up (SD)	−2.5	−2.2	−2.1	−1.4	−2.4	−3.3	−2.0	−2.5	−2.3	−2.0
OFC at last follow-up (SD)	−4.3	−3.5	−4.0	−3.2	−4.5	−6	−4.6	−4	−5.4	−5.2
Mental retardation	Severe	Moderate	Severe	Severe	Severe	Moderate	Severe	Moderate	Severe	Severe
Development (month)										
Holding one's head	6	4	4	5	3	4	6	4	+	3
Sitting	−	9	−	−	12	9	12	15	−	22
Walking	−	−	−	−	36	30	−	−	−	−
Speech	−	−	−	−	−	−	−	A few words spoken	−	−
Muscular hypotonia	+	+	−	−	−	NA	+	−	+	+
Seizure	−	−	−	−	−	−	−	−	+	+
EEG	Spike and slow	NP	Normal	NP	Normal	Normal	Normal	Normal	Spike	Abnormal
MRI[a]	CE, ME, PO	CE, ME, PO	CE, ME, PO	CE, ME, PO	CE, ME, PO	CE, ME[b], PO[b]	CE, ME, PO	CE, ME, PO	CE, ME, PO	CE, ME, PO
Other abnormalities	Bilateral sensory deafness	Craniofacial dysmorphisms, bilateral hydronephrosis, deafness					Bilateral sensory deafness		Severe scoliosis	
Karyotype	46,XX	46,XX	46,XX	46,XX, inv (9)(p12q13)[c]	46,XX	46,XX	46,XX	46,XX	46,XX	46,XX
X-tiling array	NP	NP	−	NP	−	−	del(X) (p11.3p11.4)dn	del(X) (p11.3p11.4)dn	dup(X)(p11.4)	dup(X) (p11.4), dup(X) (p11.21)
Size of CNV (Mb)							3.0	1.1	0.2	Two times 0.2

Table 1 continued

Patient	1	2	3	4	5	6	7	8	9	10
CASK mutation										
Exon	2	4	27	3	Intron 4	Intron 21				
Nucleotide change	c.79C>T	c.316C>T	c.2632C>T	c.243_244delTA	c.357-1G>A	c.2040-1G>C	None	NP	NP	NP
Protein change	p.R27X	p.R106X	p.Q878X	p.Y81X	p.S119Rfs7X p.H120Pfs22X	p.W680Cfs29X p.W680Cfs1X				
CASK aberration in parents	NP	None	None	NP	None	None	None	None	NP	None

NA not available, *NP* not performed, *SD* standard deviation

+, present; −, absent

[a] Showing hypoplastic region: *CE* cerebellum, *ME* mesencephalon, *PO* pons

[b] The hypoplasia is mild

[c] Normal variation

using genomic DNA of patient 10, four unaffected females and one unaffected male using the 7500 Real-Time PCR System (Applied Biosystems) and KAPA SYBR® FAST qPCR Master Mix (KAPA Biosystems) according to the manufacturers' instructions. Primers were designed using Primer3 software. Four primer combinations, Primer 1–4, were designed for the duplication at Xp11.4 between A_16_P21451772 and A_16_P21451795, which were oligonucleotides on the nucleotide array. Six primer combinations, primer 5–10, were designed for the duplication at Xp11.21 between A_16_P03708491 and A_14_P101900. The sequences of the primer combinations are provided in Supplementary Table 2.

Results

Mutation analysis

The analysis detected the mutations probably responsible for the phenotypes in six cases (Table 1; Fig. 2). Nonsense mutations were detected in three cases: c.79C>T (*p.R27X*), c.316C>T (*p.R106X*) and c.2632C>T (*p.Q878X*) in patients 1, 2 and 3, respectively. A deletion of two nucleotides in exon 3 was detected in patient 4: c.243_244delTA (*p.Y81X*). Mutations in intron were detected in two cases: c.357-1G>A of intron 4 in patient 5 and c.2040-1G>C of intron 21 in patient 6. Both intronic mutations were located at the splice acceptor sites and possibly affected the splicing of *CASK*. None of the mutations has been reported previously (Najm et al. 2008; Tarpey et al. 2009). In patients 2, 3, 5 and 6, we did not detect the mutation in either of the parents (data not shown), suggesting the mutations to be de novo.

aCGH analysis and FISH

In four patients without possible causative mutations in *CASK*, CNVs involving *CASK* were detected by aCGH (Table 1; Fig. 3a). Heterozygous deletions including the gene were detected in patients 7 and 8. Duplications were detected in two patients: a 0.2-Mb intragenic duplication within *CASK* was detected in patient 9, and two 0.2-Mb duplications were detected at Xp11.4 within *CASK* and at Xp11.21, including part of *AX747041*, the function of which was unclear, in patient 10. All the CNVs were confirmed by FISH (Fig. 3b). Notably, FISH demonstrated that the duplication was a tandem duplication in patient 9, and that the two duplications in patient 10 were caused by a paracentric inversion between Xp11.4 and Xp11.21. In patients 7, 8 and 10, FISH detected the same CNV in neither of the parents, suggesting the CNVs to be de novo (data not shown). Parental samples of patient 9 were not

Fig. 1 Representative brain MRI scans in six patients. All of them showed a hypoplastic cerebellum, mesencephalon and pons
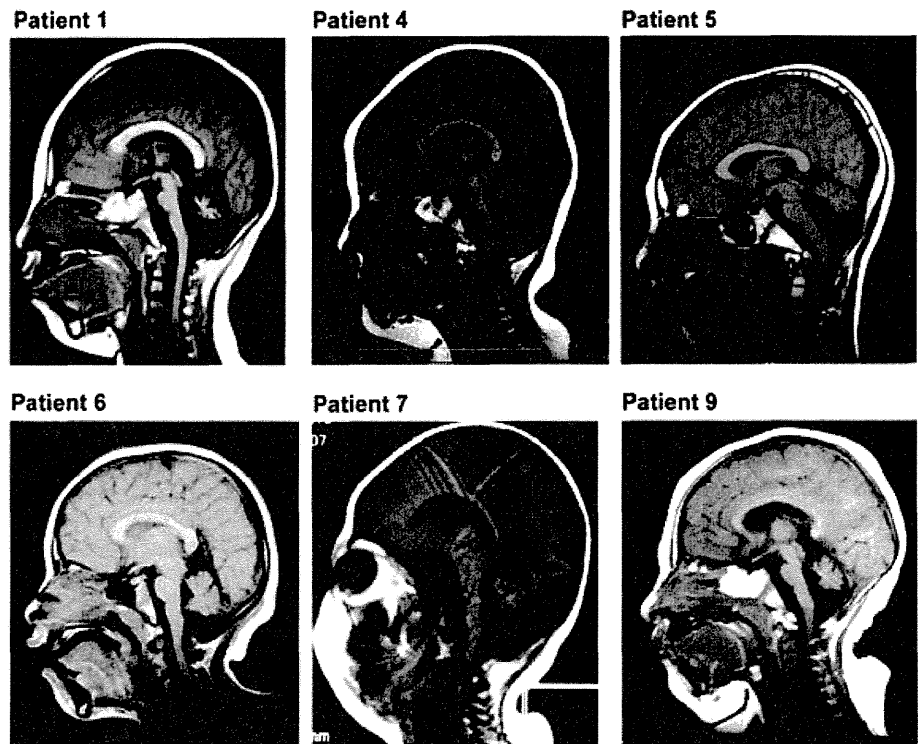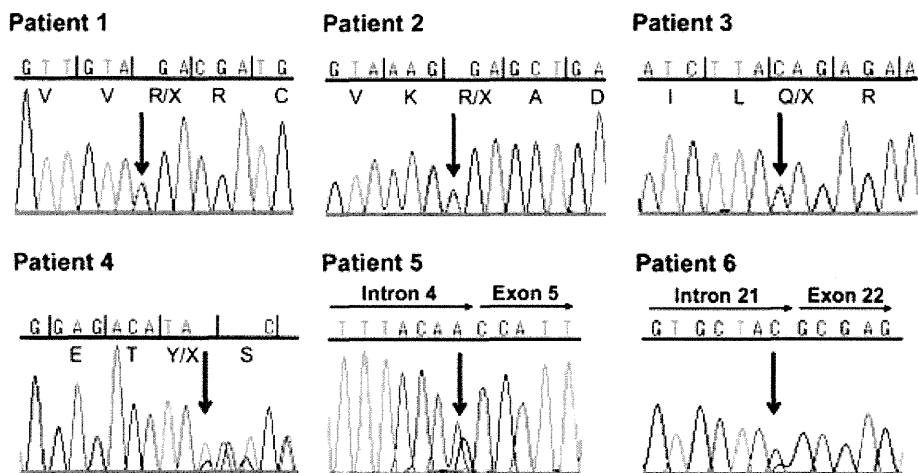

Fig. 2 Partial electropherograms depicting the CASK mutations; c.79C>T in patient 1, c.316C>T in patient 2, c.2632C>T in patient 3, c.243_244delTA in patient 4, c.357-1G > A in patient 5 and c.2040-1G > C in patient 6. Each *arrow* indicates the mutated nucleotide. The translated amino acid sequences are shown under the nucleotides. The *black vertical lines* indicate reading frames

available. A scheme of the deletions and duplications is shown in Fig. 3c.

Transcript analysis

Subsequently, we estimated the effect of the mutations at the splicing acceptor sites. For patient 5, we performed RT-PCR using primer combinations designed to target the area between exon 3 and exon 8 and obtained two products;

one was the same size as the wild-type amplicon and the other was a smaller product (Fig. 4a; Supplemental Table 1). The smaller product was cloned and sequenced to show three different-sized transcripts (clone 1–3, Fig. 4b). Clone 1 was a transcript missing all of exon 5 (Fig. 4c) and clone 3 was a transcript in which exon 5 was absent and alternatively a part of intron 5 was inserted (Fig. 4d). Both were aberrant CASK transcripts leading to a frameshift and a premature stop codon, *p.S119Rfs7X and p.H120Pfs22X,*

respectively (Table 2). Clone 2 was a normal transcript. For patient 6, we also performed RT-PCR using primer combinations designed between exon 19 and exon 27 to obtain a smaller product than the control (Fig. 5a; Supplemental Table 1). The product was cloned and sequenced to show transcripts of three different sizes (clone 1–3, Fig. 5b). Clone 1 was a transcript without the initial 8 bp of exon 22 (Fig. 5c) and clone 3 was a transcript missing all of exon 22 (Fig. 5d). Both were aberrant *CASK* transcripts leading to a frameshift and a premature stop codon, *p.W680Cfs29X* and *p.W680Cfs3X*, respectively (Table 2). Clone 2 was a normal transcript; therefore, both of the mutations at the splicing acceptor sites caused *CASK* null mutations.

We also estimated the effects of the duplication of *CASK* in patients 9 and 10. Since the results of FISH suggested that an interstitial part of *CASK* was duplicated in patient 9 (Fig. 3b), we precisely mapped the duplication using the oligonucleotide array (Fig. 6a). We predicted the structure of the intragenic duplication and performed RT-PCR using primer combinations designed between exon 7 and exon 4, that is, specific to the duplication, and obtained a product (Fig. 6; Supplementary Fig. 1a; Supplementary Table 1). Sequencing showed the product of the RT-PCR to consist of exon 7 followed by exon 3 (Fig. 6c). These results indicated that the duplication in patient 9 probably caused an aberrant *CASK* transcript leading to a frameshift and a premature stop codon.

In patient 10, FISH suggested that the duplications were a result of a paracentric inversion (Fig. 3b). We also determined the precise size of each duplication with an oligonucleotide array (Fig. 7a) and qPCR (Supplementary Fig. 1b) and predicted a rearrangement in which exon 1, exon 2 and the duplicated exons 3–9 of *CASK* were at Xp11.21. (Fig. 7b). Inversion-specific genomic PCR using a primer combination between intron 8 of *CASK* and intron 1 of *AX747041* supported such a rearrangement (Fig. 7c; Supplementary Table 1). They were potentially transcribed to produce an aberrant transcript with exon 2 of *AX747041* which was originally located at Xp11.21 (Fig. 7b); thus, an inversion-specific RT-PCR using primer combinations targeting between exon 7 of *CASK* and exon 2 of *AX747041* was performed and a product was generated only in patient 10 (Fig. 7d; Supplementary Table 1). Sequencing of this product demonstrated that following exon 9 of *CASK*, exon 2 of *AX747041* was transcribed to produce a stop codon (Fig. 7e). These results clearly proved that the inverted duplication in patient 10 also resulted in *CASK* null mutations.

Discussion

Among the ten cases with phenotypic criteria, female, MR and MICPCH, we detected genomic aberrations of *CASK*

Fig. 3 Array-CGH analysis and FISH. **a** Results of the X-array analyses. Clones are ordered according to the UCSC mapping position. Each *spot* represents the test/reference value after normalization and $\log_2$ transformation in each BAC clone. The *gray* vertical bar indicates the position of a centromere. *Black arrows* indicate each CNV. An approximately 3.0-Mb deletion at Xp11.4p11.3 was detected in patient 7 and an approximately 1.1-Mb deletion at Xp11.4p11.3 was detected in patient 8. In patient 9, an approximately 0.2-Mb duplication at Xp11.4 was detected based on the increased ratios of one BAC clone. In patient 10, two approximately 0.2-Mb duplications were detected at Xp11.4 and at Xp11.21. **b** Representative results of FISH and enlarged X chromosomes in each patient. *Yellow arrows* denote aberrant signal(s). Of the enlarged chromosomes, the *left* one is intact and the right one is affected, and *white* bands indicate the position of the centromere. In patients 7 and 8, FISH using a probe at Xp11.4 (RP11-95C16, *red*) and a reference probe at Xq28 (RP11-119A22, *green*) confirmed each deletion (*yellow arrow*). In patient 9, FISH using a probe at Xp11.4 (RP11-1069J5, *red*) and the same reference probe delineated tandem duplication (*yellow arrow*). In patient 10, both probes at the two duplications, RP11-1069J5 (*red*) and RP11-1106F5 (*green*), were hybridized at the same position (two *yellow arrows* in the *left enlarged panel*). On the right side, a schematic representation is shown. In the *right enlarged panel*, the probe combination located within the two duplications, RP11-95C16 at Xp11.4 (*red*) and RP11-179I23 at Xp11.21 (*green*), showed an inverted orientation in the affected chromosome X (two *yellow arrows*, *right*) compared with the intact chromosome X (*left*). On the right, a schematic representation is shown. **c** Scheme of the region around *CASK*, BAC clones, genes, deletions and duplications. *Open double-headed arrows* indicate the deletions and *filled double-headed arrows* indicate the duplications. *Horizontal black bars* indicate BAC clones (RP-11 series). *Thin horizontal arrows* indicate genes and their directions. In concordance with ISCN 2005 (Shaffer and Tommerup 2005), this result was described as follows: patient 7, arr cgh Xp11.4p11.3(RP11-829G10 → RP11-469F12)x1; patient 8, arr cgh Xp11.4p11.3(RP11-1069J5 → RP11-52P6)×1; patient 9, arr cgh Xp11.4(RP11 → 1069J5)x3; and patient 10, arr cgh Xp11.4 (RP11-1069J5)×3,Xp11.21(RP11-5415 → RP11-1106F5)×3 (color figure online)

in all cases, nonsense mutations in three cases, a 2 bp-deletion in one case, mutations at the splice acceptor sites in two cases, heterozygous deletions encompassing *CASK* in two cases and intragenic duplications in two cases. Not only the nonsense mutations but also mutations at the splice acceptor sites generated aberrant *CASK* transcripts, leading to a frameshift and a premature stop codon. The intragenic tandem duplication in patient 9 and the intragenic inversion/duplication probably due to inv(X) (p11.4p11.21) in patient 10 also produced an aberrant transcript causing a frameshift, leading to a premature stop codon within *CASK*. We previously reported that the heterozygous deletion containing *CASK* probably reduced the expression of intact *CASK* in a female patient (Hayashi et al. 2008). The current study extends the variety of genomic alterations causing *CASK* null mutations. The incidence of *CASK* mutations and of CNVs involving *CASK* was almost the same, and there was no mutational hot spot in *CASK* according to a previous report (Najm
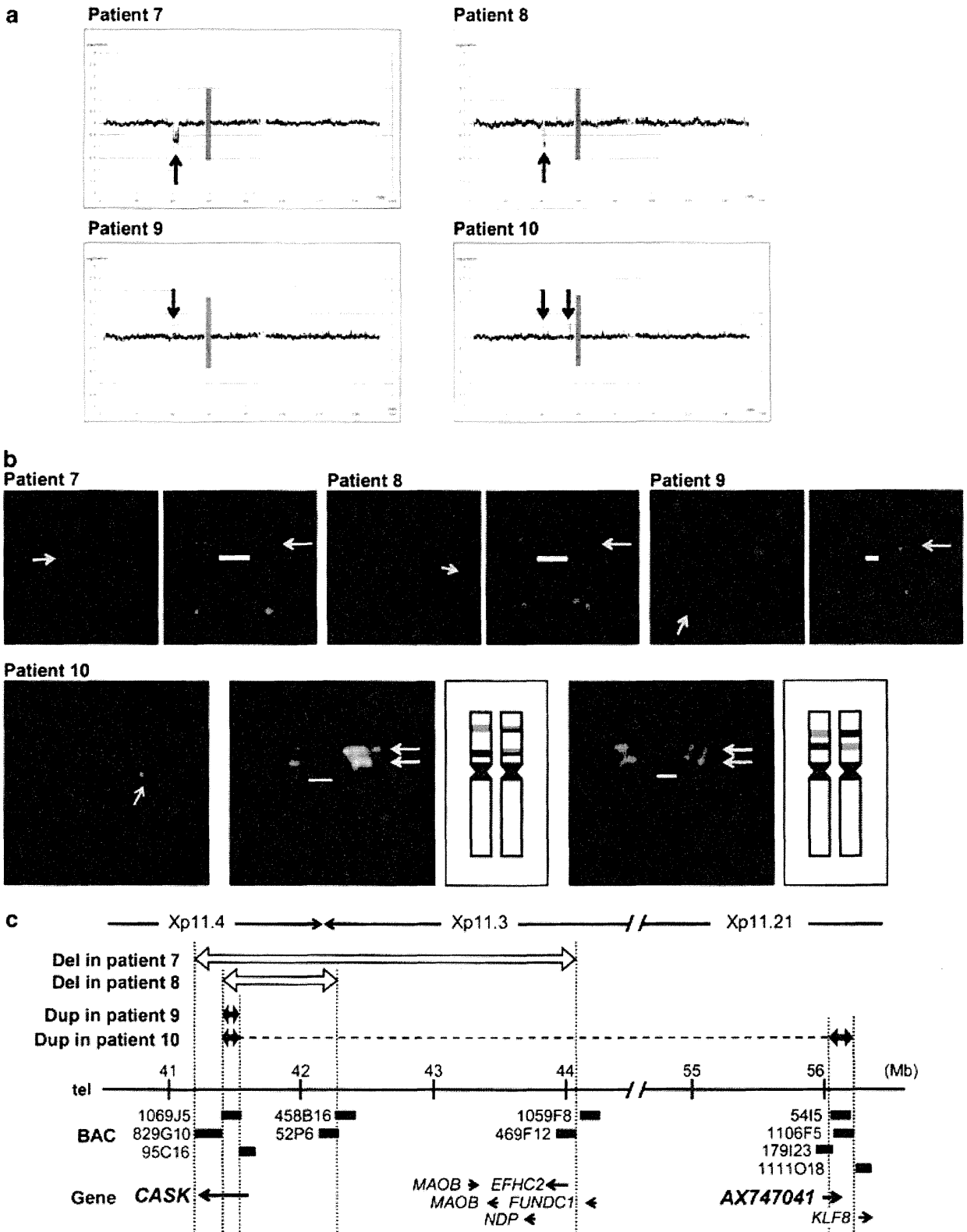
Fig. 4 Exon skipping and aberrant transcripts in patient 5. **a** RT-PCR using primer combinations for exons 3 and 8. The *arrow* indicates an aberrant-sized product in patient 5. *M* marker: φX174 RF DNA/Hae III Fragments. *P5* patient 5. *C* control. *N* negative control, no DNA added. **b** The PCR products were cloned to reveal clones of three sizes. Representative clones are shown. No. 1 and no. 3 are aberrant-sized clones and no. 2 is a normal-sized clone. **c**, **d** Sequence chromatograms from clones 1 and 3. In clone 1, exon 5 was skipped to cause an aberrant transcript leading to a frameshift and a premature stop codon in exon 6 (**c**). In clone 3, next to exon 4, exons 5 and 6 were skipped and part of intron 5 was inserted to cause an aberrant transcript leading to a frameshift and a premature stop codon in intron 5 (**d**). The translated amino acid sequences are shown under the nucleotides and *underlines* indicate the frameshift mutations. The *black vertical lines* indicate reading frames. *Dashed vertical lines* denote exon–exon or exon–intron boundaries
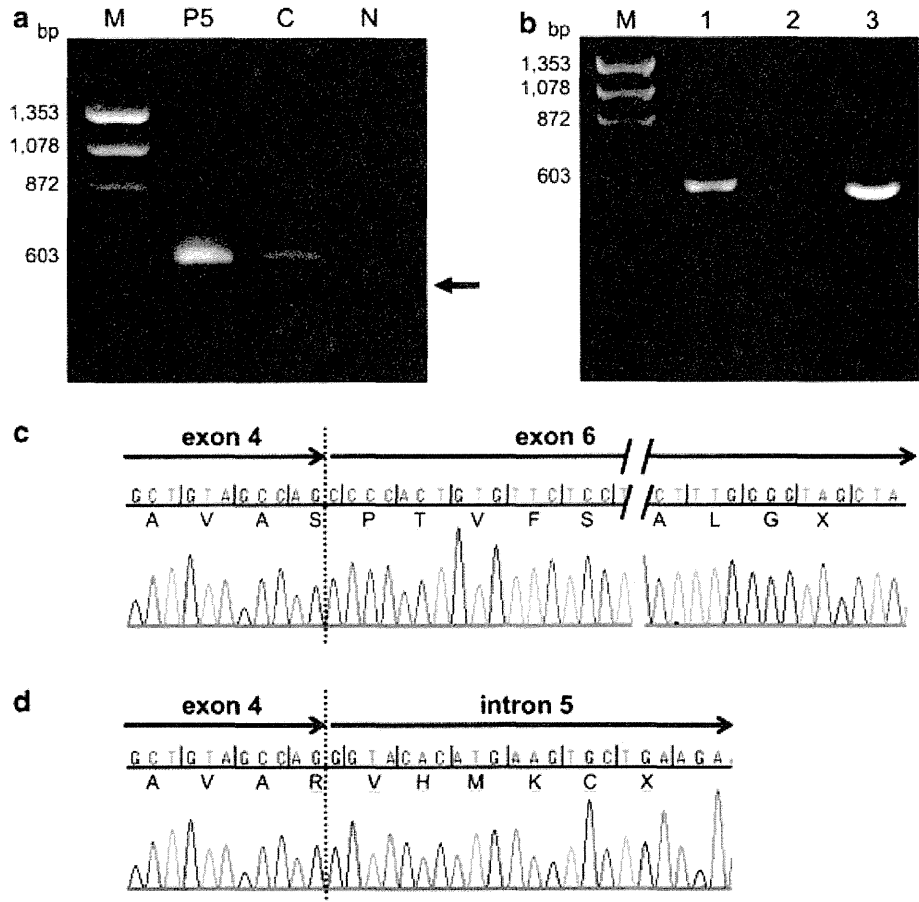
et al. 2008) and ours. The molecular mechanism causing the recurrent CNVs remains unclear. For example, known low-copy repeats (LCRs), important factors facilitating nonallelic homologous recombination (NAHR) (Stankiewicz and Lupski 2002), do not adequately explain the CNVs, since no LCRs on/around breakpoints involved in CNVs in any of the current four cases and our previous case (Hayashi et al. 2008) have been registered, even in up-to-date genome databases (UCSC March 2006 and February 2009 build). While the CNVs may be incidental, detailed analyses of the DNA sequence flanking the breakpoints of the CNVs may reveal the mechanisms behind the genomic rearrangement around *CASK* (Inoue et al. 2002).

Recently, *CASK* aberrations have been reported in patients with MR with/without MICPCH (Hsueh 2009) (Table 2). As previously mentioned, a heterozygous nonsense mutation and a disruption caused by a chromosomal inversion were detected in females with severe MR and

MICPCH (Najm et al. 2008). They also reported a synonymous mutation causing exon 9 to be skipped in a male, who died at 2 weeks of age. On the other hand, through mutational screening of X-linked MR, four missense mutations of *CASK* were found in male patients with MR (Tarpey et al. 2009). Their MR was mild and two also revealed nystagmus. Moreover, a missense mutation of *CASK* was identified in a family with FG syndrome (Piluso et al., 2009). These reports suggest that *CASK* aberrations cause three very different phenotypes: severe MR with MICPCH in females, mild MR in males and FG syndrome in males, depending on the type of aberration. As *Cask* knockout (KO) mice were reported to die in the neonatal period (Laverty and Wilson 1998; Atasoy et al. 2007), a complete lack of *CASK* is probably lethal, consistent with the male patient with the *CASK* mutation (Najm et al. 2008); however, missense mutations in male patients probably cause different clinical conditions, i.e., mild MR or FG syndrome (Tarpey et al. 2009; Piluso et al. 2009), and haploinsufficiency of

Table 2 Summary of mutations affecting single or few base pairs in the CASK gene

Gender	Phenotype	Type of mutation	Nucleotide change	Protein change	Comment	Report
F	MR/MICPCH	Nonsense	c.1915C>T	p.R639X		Najm et al. 2008
M	MR/MICPCH	Synonymous	c.915G > A	p.=	Skipping of exon 9 observed; the patient died at 2 weeks	Najm et al. 2008
F	MR/MICPCH	Nonsense	c.79C>T	p.R27X		Our case (patient 1)
F	MR/MICPCH	nonsense	c.316C>T	p.R106X		Our case (patient 2)
F	MR/MICPCH	Nonsense	c.2632C>T	p.Q878X		Our case (patient 3)
F	MR/MICPCH	ins/del	c.243_244delTA	p.Y81X		Our case (patient 4)
F	MR/MICPCH	Splice-site mutation	c.357-1G>A	p.S119Rfs7X p.H120Pfs22X	Skipping of exon 5, or skipping of exon 5 and insertion of partial intron 5	Our case (patient 5)
F	MR/MICPCH	Splice-site mutation	c.2040-1G>C	p.W680Cfs29X p.W680Cfs3X	Skipping of partial or entire exon 22	Our case (patient 6)
M	FG syndrome	Missense	c.83G>T	p.R28L	Skipping of exon 2 observed with low frequency	Piluso et al. 2009
M	Mild MR	Missense	c.2129A>G	p.D710G		Tarpey et al. 2009
M	Mild MR	Missense	c.802T>C	p.Y268H		Tarpey et al. 2009
M	Mild MR	Missense	c.2767C>T	p.W914R		Tarpey et al. 2009
M	Mild MR	Missense	c.1186C>T	p.P396S		Tarpey et al. 2009

Fig. 5 Exon skipping and aberrant transcripts in patient 6. **a** RT-PCR using primer combinations for exons 19 and 27. The *arrow* indicates an aberrant-sized product in patient 6. *M* marker, φX174 RF DNA/Hae III Fragments, *P6* patient 6, *C* control, *N* negative control. **b** The PCR products were cloned to reveal clones of three sizes. Representative clones are shown. No. 1 and 3 are aberrant-sized clones and no. 2 is a normal clone. **c, d.** Sequence chromatograms from clone 1 and 3. In clone 1, the initial 8 bp of exon 22 was absent, causing an aberrant transcript leading to a frameshift and a premature stop codon (**c**). In clone 3, all of exon 22 was missing, resulting in an aberrant transcript leading to a frameshift and a premature stop codon in exon 23 (**d**). The translated amino acid sequences are shown under the nucleotides and *underlines* indicate the frameshift mutations. The *black vertical lines* indicate reading frames. Dashed vertical lines denote exon–exon boundaries
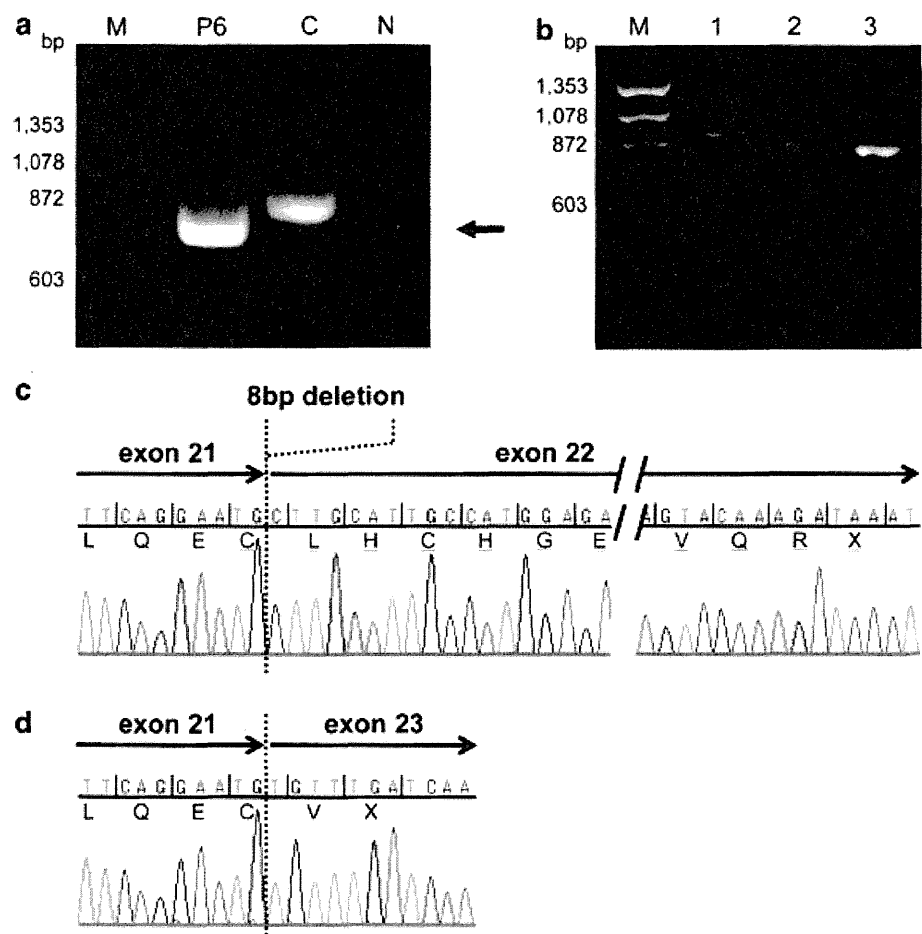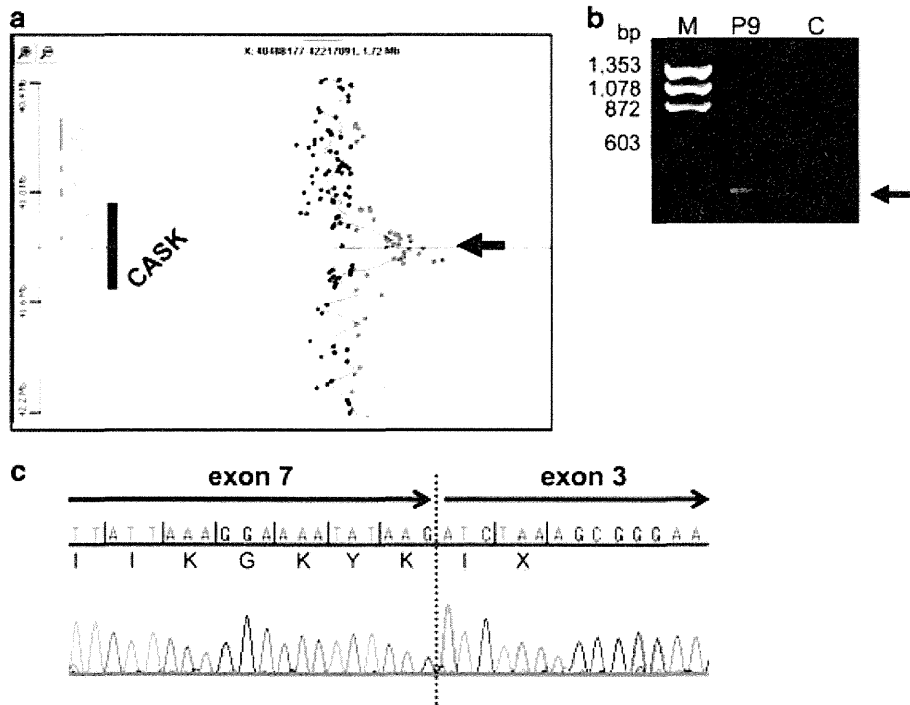
Fig. 6 Analsyses of the duplication in patient 9. **a** Results obtained with Agilent Human Genome CGH microarray kit 244K. This result was described as follows: arr Xp11.4(41,280,790-41,439,415)×3. The duplication included exon 3–7 of *CASK*. It was unclear whether exon 8 was included (*arrow*). The relevant genes are emphasized. **b.** RT-PCR using primer combinations for exon 7 and 4. A product was gained only from patient 9 (*arrow*). *M* marker: φX174 RF DNA/Hae

III Fragments, *P9* patient 9, *C* control. **c.** Chromatograms for the RT-PCR product shown in (**b**). Next to exon 7, the duplicated exon 3 was transcribed to cause an aberrant transcript leading to a frameshift and a premature stop codon. The translated amino acid sequences are shown under the nucleotides and *underlines* indicate the frameshift mutations. The *black vertical lines* indicate reading frames. *Dashed vertical lines* denote exon–exon boundaries

CASK in females probably causes severe MR with MIC-PCH (Hayashi et al. 2008; Najm et al. 2008).

CASK encodes a multi-domain scaffolding protein with several critical roles in brain development and synaptic functions, including synaptic interaction, neurotransmitter release and dendritic spine formation (Hata et al. 1996; Irie et al. 1997; Cohen et al. 1998; Hsueh et al. 2000; Olsen et al. 2005; Hsueh 2006; Chao et al. 2008). CASK also regulates the expression of *RELN* involved in brain development through interactions with Tbr-1 via a guanylate kinase (GK)-like domain (Hsueh et al. 2000), and this function may be essential for the etiology of MR with MICPCH. *RELN* plays an important role in neural migration and brain development (D'Arcangelo et al. 1995; Ogawa et al. 1995; Rice et al. 1998), and its mutation is associated with lissencephaly with cerebellar hypoplasia (Hong et al. 2000). While the current analysis provides novel mutations and several types of genomic aberrations of *CASK* causing MR with MIC-PCH, except for the heterozygous deletions all the muta-

tions and duplications produced aberrant transcripts which will be degraded due to nonsense-mediated mRNA decay and no CASK proteins will be expressed from the mutant alleles; that is, they cause *CASK* null mutations. This may explain the similarity of the phenotypes of MR with MICPCH regardless of the type of *CASK* aberration. The relation between genotypic variety and phenotypic similarity could be clinically useful for detecting and investigating potential patients with *CASK* aberrations.

Web Resources. URLs of the Web sites referred to in this manuscript are as follows:UCSC Genome Bowser, http://genome.ucsc.edu/ (March 2006 build)NCBI, http://www.ncbi.nlm.nih.gov/Online Mendelian Inheritance in Man (OMIM), http://www.ncbi.nlm.nih.gov/Omim/Primer3, http://frodo.wi.mit.edu/primer3/.

Accession Numbers. The *CASK* genomic region is from The UCSC March 2006 build (NCBI36/hg18), range = chrX:41259133-41667231. The GenBank accession number of the human CASK cDNA transcript variant 1 (isoform 1)
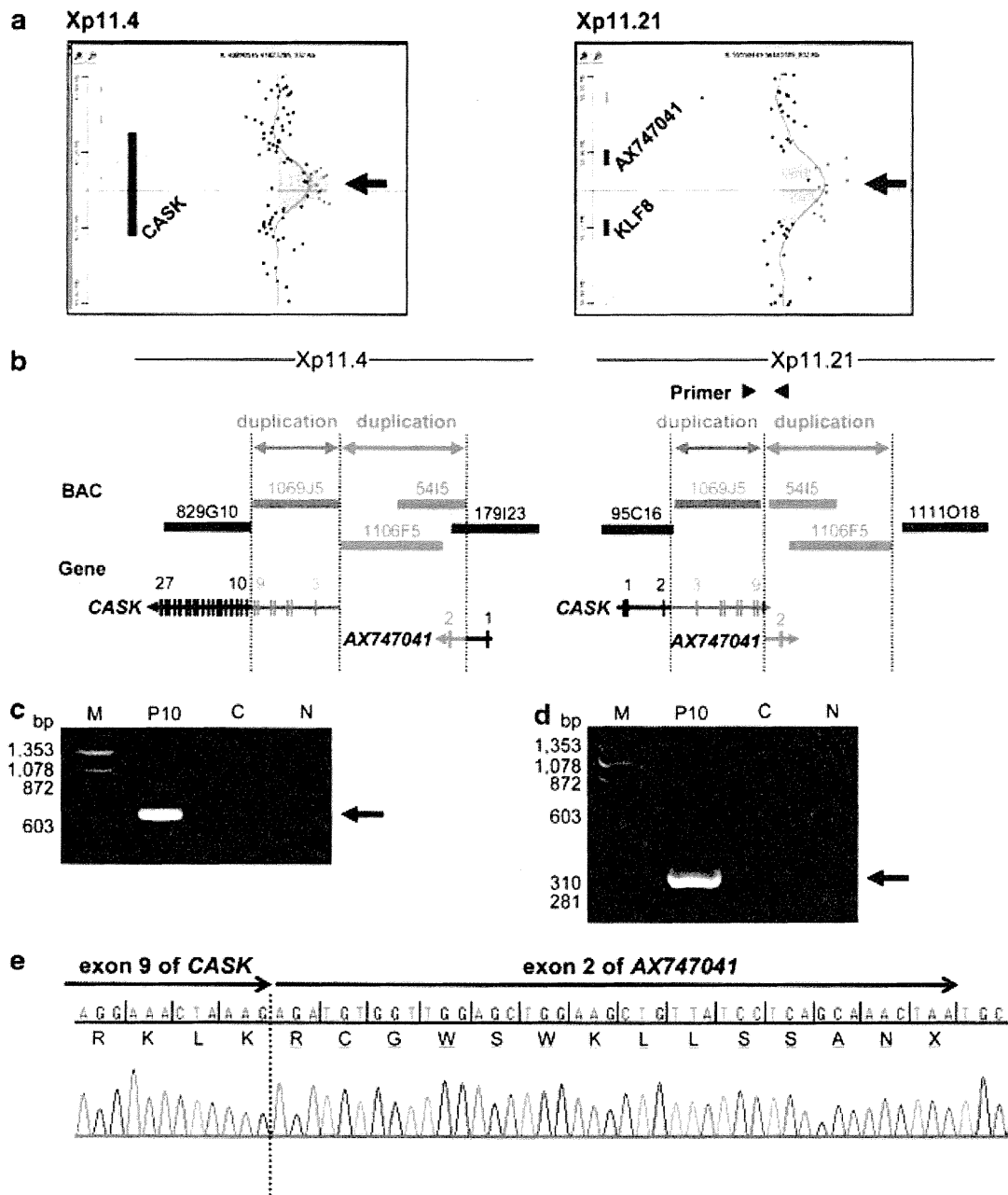
a Xp11.4   Xp11.21

b ————Xp11.4————   ————Xp11.21————

Primer ▶ ◀

duplication duplication   duplication duplication

BAC 829G10 1069J5 5415 179123   95C16 1069J5 5415 1111O18
1106F5   1106F5

Gene
27 10 9 3   1 2 3 9
CASK ◀▓▓▓▓▓▓▓▓ ┤├ ┤├ ┤├   CASK ●─┤├ ┤├ ┤├ ┤├
2 1   2
AX747041 ◀┤├   AX747041 ◀├▷

c bp M P10 C N   **d** bp M P10 C N
1,353   1,353
1,078   1,078
872   872
603 ←   603
310 ←
281

e exon 9 of CASK   exon 2 of AX747041

A G G A A C T A A G A G A T G T G G T T G G A G C T G G A A G C T G T T A T C C T C A G C A A C T A A T G C
R K L K R C G W S W K L L S S A N X

Fig. 7 Analyses of the duplications in patient 10. a Results obtained with Agilent Human Genome CGH microarray kit 244K. This result was described as follows: arr Xp11.4(41,381,483-41,539,961)×3, arr Xp11.21(56,022,198-56,272,783)×3. The duplication at Xp11.4 included exons 3–8 of CASK (arrow, left panel) and the duplication at Xp11.21 included exon 2 of AX747041 (arrow, right panel). The relevant genes are emphasized. b A predicted structure of two duplications in patient 10 based on the results of FISH, oligonucleotide array and qPCR. The region denoted by gray double-headed arrows, originally at Xp11.4 and including exons 3–9 of CASK, was inverted and duplicated at Xp11.21. The region denoted by red double-headed arrows, originally at Xp11.21 and including exon 2 of AX747041, was inverted and duplicated at Xp11.4. Exons 1 and 2 of CASK and exon 1 of AX747041 are also involved in the inversion but not duplicated. Vertical lines denote exons and arrows indicate the direction of CASK and

AX747041, respectively. Numbers above the genes denote exons. Horizontal thick bars indicate BAC clones (RP-11 series). A pair of black triangles indicates the primer combinations for inversion-specific genomic PCR. c Inversion-specific PCR revealed a product only in patient 10 (arrow). M marker; φX174 RF DNA/Hae III Fragments, P10 patient 10, C control, N negative control. d Inversion-specific RT-PCR also revealed a product only in patient 10 (arrow). M marker: φX174 RF DNA/Hae III Fragments, P10 patient 10, C control, N negative control. e Sequence chromatograms from the RT-PCR product shown in (d). Next to exon 9 of CASK, exon 2 of AX747041 was transcribed to cause an aberrant transcript leading to a frameshift and a premature stop codon. The translated amino acid sequences are shown under the nucleotides and underlines indicate the frameshift mutations. The black vertical lines indicate reading frames. Dashed vertical lines denote exon–exon boundaries (color figure online)

⌐ Springer

and the human CASK protein isoform 1 are NM_003688.3 and NP_003679.2, respectively.

References

Atasoy D, Schoch S, Ho A, Nadasy KA, Liu X, Zhang W, Mukherjee K, Nosyreva ED, Fernandez-Chacon R, Missler M, Kavalali ET, Südhof TC (2007) Deletion of CASK in mice is lethal and impairs synaptic function. Proc Natl Acad Sci USA 104:2525–2530

Chao HW, Hong CJ, Huang TN, Lin YL, Hsueh YP (2008) SUMOylation of the MAGUK protein CASK regulates dendritic spinogenesis. J Cell Biol 182:141–155

Cohen AR, Woods DF, Marfatia SM, Walther Z, Chishti AH, Anderson JM (1998) Human CASK/LIN-2 binds syndecan-2 and protein 4.1 and localizes to the basolateral membrane of epithelial cells. J Cell Biol 142:129–138

D'Arcangelo G, Miao GG, Chen SC, Soares HD, Morgan JI, Curran T (1995) A protein related to extracellular matrix proteins deleted in the mouse mutant reeler. Nature 374:719–723

Hata Y, Butz S, Südhof TC (1996) CASK: a novel dlg/PSD95 homolog with an N-terminal calmodulin-dependent protein kinase domain identified by interaction with neurexins. J Neurosci 16:2488–2494

Hayashi S, Kurosawa K, Imoto I, Mizutani S, Inazawa J (2005) Detection of cryptic chromosome aberrations in a patient with a balanced t(1;9)(p34.2;p24) by array-based comparative genomic hybridization. Am J Med Genet A 139:32–36

Hayashi S, Honda S, Minaguchi M, Makita Y, Okamoto N, Kosaki R, Okuyama T, Imoto I, Mizutani S, Inazawa J (2007) Construction of a high-density and high-resolution human chromosome X array for comparative genomic hybridization analysis. J Hum Genet 52:397–405

Hayashi S, Mizuno S, Migita O, Okuyama T, Makita Y, Hata A, Imoto I, Inazawa J (2008) The CASK gene harbored in a deletion detected by array-CGH as a potential candidate for a gene causative of X-linked dominant mental retardation. Am J Med Genet A 146A:2145–2151

Hong SE, Shugart YY, Huang DT, Shahwan SA, Grant PE, Hourihane JO, Martin ND, Walsh CA (2000) Autosomal recessive lissencephaly with cerebellar hypoplasia is associated with RELN mutations. Nat Genet 26:93–96

Hsueh YP (2006) The role of the MAGUK protein CASK in neural development and synaptic function. Curr Med Chem 13:1915–1927

Hsueh YP (2009) Calcium/calmodulin-dependent serine protein kinase and mental retardation. Ann Neurol 66:438–443

Hsueh YP, Wang TF, Yang FC, Sheng M (2000) Nuclear transcription and transcription regulation by the membrane-associated guanylate kinase CASK/LIN-2. Nature 404:298–302

Inazawa J, Inoue J, Imoto I (2004) Comparative genomic hybridization (CGH)-arrays pave the way for identification of novel cancer-related genes. Cancer Sci 95:559–563

Inoue K, Osaka H, Thurston VC, Clarke JT, Yoneyama A, Rosenbarker L, Bird TD, Hodes ME, Shaffer LG, Lupski JR (2002) Genomic rearrangements resulting in PLP1 deletion occur by nonhomologous end joining and cause different dysmyelinating phenotypes in males and females. Am J Hum Genet 71:838–853

Irie M, Hata Y, Takeuchi M, Ichtchenko K, Toyoda A, Hirao K, Takai Y, Rosahl TW, Südhof TC (1997) Binding of neuroligins to PSD-95. Science 277:1511–1515

Laverty HG, Wilson JB (1998) Murine CASK is disrupted in a sex-linked cleft palate mouse mutant. Genomics 53:29–41

Najm J, Horn D, Wimplinger I, Golden JA, Chizhikov VV, Sudi J, Christian SL, Ullmann R, Kuechler A, Haas CA, Flubacher A, Charnas LR, Uyanik G, Frank U, Klopocki E, Dobyns WB, Kutsche K (2008) Mutations of CASK cause an X-linked brain malformation phenotype with microcephaly and hypoplasia of the brainstem and cerebellum. Nat Genet 40:1065–1067

Ogawa M, Miyata T, Nakajima K, Yagyu K, Seike M, Ikenaka K, Yamamoto H, Mikoshiba K (1995) The reeler gene-associated antigen on Cajal-Retzius neurons is a crucial molecule for laminar organization of cortical neurons. Neuron 14:899–912

Olsen O, Moore KA, Fukata M, Kazuta T, Trinidad JC, Kauer FW, Streuli M, Misawa H, Burlingame AL, Nicoll RA, Bredt DS (2005) Neurotransmitter release regulated by a MALS-liprin-alpha presynaptic complex. J Cell Biol 170:1127–1134

Piluso G, D'Amico F, Saccone V, Bismuto E, Rotundo IL, Di Domenico M, Aurino S, Schwartz CE, Neri G, Nigro V (2009) A missense mutation in CASK causes FG syndrome in an Italian family. Am J Hum Genet 84:162–177

Rice DS, Sheldon M, D'Arcangelo G, Nakajima K, Goldowitz D, Curran T (1998) Disabled-1 acts downstream of Reelin in a signaling pathway that controls laminar organization in the mammalian brain. Development 125:3719–3729

Saito-Ohara F, Fukuda Y, Ito M, Agarwala KL, Hayashi M, Matsuo M, Imoto I, Yamakawa K, Nakamura Y, Inazawa J (2002) The Xq22 inversion breakpoint interrupted a novel Ras-like GTPase gene in a patient with Duchenne muscular dystrophy and profound mental retardation. Am J Hum Genet 71:637–645

Shaffer LG, Tommerup N (2005) An International System for Human Cytogenetic Nomenclature (2005). Karger, Basel

Stankiewicz P, Lupski JR (2002) Genome architecture, rearrangements and genomic disorders. Trends Genet 18:74–82

Stevenson D, Laverty HG, Wenwieser S, Douglas M, Wilson JB (2000) Mapping and expression analysis of the human CASK gene. Mammalian Genome 11:934–937

Tarpey PS, Smith R, Pleasance E, Whibley A, Edkins S, Hardy C, O'Meara S, Latimer C, Dicks E, Menzies A, Stephens P, Blow M, Greenman C, Xue Y, Tyler-Smith C, Thompson D, Gray K, Andrews J, Barthorpe S, Buck G, Cole J, Dunmore R, Jones D, Maddison M, Mironenko T, Turner R, Turrell K, Varian J, West S, Widaa S, Wray P, Teague J, Butler A, Jenkinson A, Jia M, Richardson D, Shepherd R, Wooster R, Tejada MI, Martinez F, Carvill G, Goliath R, de Brouwer AP, van Bokhoven H, van Esch H, Chelly J, Raynaud M, Ropers HH, Abidi FE, Srivastava AK, Cox J, Luo Y, Mallya U, Moon J, Parnau J, Mohammed S, Tolmie JL, Shoubridge C, Corbett M, Gardner A, Haan E, Rujirabanjerd S, Shaw M, Vandeleur L, Fullston T, Easton DF, Boyle J, Partington M, Hackett A, Field M, Skinner C, Stevenson RE, Bobrow M, Turner G, Schwartz CE, Gecz J, Raymond FL, Futreal PA, Stratton MR (2009) A systematic, large-scale resequencing screen of X-chromosome coding exons in mental retardation. Nat Genet 41:535–543

ORIGINAL ARTICLE

Subtelomeric deletions of 1q43q44 and severe brain impairment associated with delayed myelination

Keiko Shimojima[1], Nobuhiko Okamoto[2], Yume Suzuki[3], Mari Saito[3], Masato Mori[3], Tatanori Yamagata[3], Mariko Y Momoi[3], Hideji Hattori[4], Yoshiyuki Okano[4], Ken Hisata[5], Akihisa Okumura[5] and Toshiyuki Yamamoto[1]

Subtelomeric deletions of 1q44 cause mental retardation, developmental delay and brain anomalies, including abnormalities of the corpus callosum (ACC) and microcephaly in most patients. We report the cases of six patients with 1q44 deletions; two patients with interstitial deletions of 1q44; and four patients with terminal deletions of 1q. One of the patients showed an unbalanced translocation between chromosome 5. All the deletion regions overlapped with previously reported critical regions for ACC, microcephaly and seizures, indicating the recurrent nature of the core phenotypic features of 1q44 deletions. The four patients with terminal deletions of 1q exhibited severe volume loss in the brain as compared with patients who harbored interstitial deletions of 1q44. This indicated that telomeric regions have a role in severe volume loss of the brain. In addition, two patients with terminal deletions of 1q43, beyond the critical region for 1q44 deletion syndrome exhibited delayed myelination. As the deletion regions identified in these patients extended toward centromere, we conclude that the genes responsible for delayed myelination may be located in the neighboring region of 1q43.
Journal of Human Genetics (2012) 57, 593–600; doi:10.1038/jhg.2012.77; published online 21 June 2012

INTRODUCTION

Submicroscopic subtelomeric chromosomal deletions have been found in 7.4% of children with moderate to severe mental retardation.[1] Some subtelomeric deletion syndromes are clinically recognizable and identified by characteristic features, whereas some others cannot be identified by such means. The recent development of molecular karyotyping using chromosomal microarray testing has revealed clear genotype–phenotype correlations and identified the critical chromosomal regions of the characteristic features of subtelomeric deletions. The most striking example is the Miller-Diecker syndrome, which has shown clear genotype–phenotype correlations.[2] Miller-Diecker syndrome is caused by the subtelomeric deletion of 17p, and is well recognized and characterized by lissencephaly and distinctive facial features,[3] which result from the involvement of the platelet-activating factor acetylhydrolase 1b regulatory subunit 1 gene (PAFAH1B1) and tyrosine 3-monooxygenase/tryptophan 5-monooxygenase-activation protein epsilon polypeptide gene (YWHAE), respectively; both these genes are located on 17p13.[3]

Several studies have investigated the critical region for 1q44 subtelomeric deletion syndrome and found that the core phenotypic

features of 1q44 subtelomeric deletion syndrome are microcephaly, abnormalities of the corpus callosum (ACC) and seizures.[4–16] Recently, Ballif et al.[17] analyzed patients with microdeletions of 1q44 and proposed certain genes that may be responsible for individual features.

We report the cases of six newly identified patients with 1q44 deletions; two with interstitial deletion of 1q44; and four with terminal deletion of 1q. As the patients with terminal deletion of 1q44 exhibited more severe phenotypes compared with the patients with interstitial deletion, the phenotypic differences would be derived from additionally deleted region of 1q43q44.

MATERIALS AND METHODS

Subjects

Six Japanese patients were diagnosed as having chromosomal deletions in the region of 1q43q44 in our ongoing study to analyze genomic copy number aberrations. This study was approved by the ethical committee of our institution. After obtaining written consents, we accumulated samples from the patients. Parental samples were also obtained to study their carrier status.

[1]Tokyo Women's Medical University Institute for Integrated Medical Sciences (TIIMS), Tokyo, Japan; [2]Department of Medical Genetics, Osaka Medical Center and Research Institute for Maternal and Child Health, Izumi, Japan; [3]Department of Pediatrics, Jichi Medical University, Shimotsuke, Japan; [4]Department of Pediatrics, Osaka City University School of Medicine, Osaka, Japan and [5]Department of Pediatrics, Juntendo University School of Medicine, Tokyo, Japan
Correspondence: Dr T Yamamoto, Tokyo Women's Medical University Institute for Integrated Medical Sciences (TIIMS), 8-1 Kawada-cho, Shinjuku-ward, Tokyo 162-8666, Japan.
E-mail: yamamoto.toshiyuki@twmu.ac.jp
Received 10 April 2012; revised 24 May 2012; accepted 25 May 2012; published online 21 June 2012

Methods

Genomic copy number was analyzed using the 244, 105 or 60 K Human Genome CGH Microarray (Agilent Technologies, Santa Clara, CA, USA) as described previously.[2] Genomic DNAs was extracted from peripheral blood using a standard method. Genomic copy number aberrations were visualized using Agilent Genomic Workbench version 5.5 (Agilent Technologies).

Fluorescence *in situ* hybridization (FISH) was performed as previously described, when metaphase spreads were available.[2] Bacterial artificial clones were selected from the UCSC genome browser (http://www.genome.ucsc.edu). Physical positions refer to the March 2009 human reference sequence. Bacterial artificial clone DNAs were extracted by an automatic DNA extraction system GENE PREP STAR PI-80X (Kurabo, Osaka, Japan).

RESULTS

Chromosomal deletions

Chromosomal microarray testing revealed aberrations in the 1q43q44 region in six patients (Figure 1). In patient 1 and 2, interstitial deletions of 1.9 and 2.2 Mb, respectively, were identified within the 1q43q44 region. In patient 1, FISH analysis confirmed the deletion (Figure 2a). Subsequent FISH analysis revealed no abnormalities in the parents of both families, indicating *de novo* deletions in both patients. Molecular karyotyping defined the aberrations as

arr 1q44(243 809 193–245 665 521) × 1 dn for patient 1 and arr 1q43q44(243 303 991–245 506 920) × 1 dn for patient 2.

In patient 3, terminal deletions of 1q43 were identified and confirmed by FISH analyses (Figure 2b). As FISH analyses for both parents showed no abnormalities, this deletion occurred as *de novo*. Molecular karyotyping of patient 3 was indicated as arr 1q43q44(242 442 098–249 250 621) × 1 dn.

In patient 4, a loss of genomic copy number at 1q43q44 and an additional gain at 5p15.33 were identified (Supplementary Figure 1). Subsequent FISH analysis confirmed an unbalanced translocation between 1q43 and 5p in patient 4 (Figures 2c–e), and no translocation was found in either parents. Consequently, the patient's unbalance translocation was determined to be *de novo* in origin. Her karyotype was 46,XX,der(1)t(1;5)(q43;p15.33).arr 1q43q44(242 223 230–249 212 668) × 1, 5p15.33(57 640–1 705 515) × 3 dn. The duplicated region of 5p was only 1.7 Mb of the terminal region.

In patient 5, terminal deletions of 1q43 were identified with a breakpoint in the v-akt murine thymoma viral oncogene homolog 3 gene (*AKT3*). The molecular karyotype was arr 1q44(243 880 099–249 212 668) × 1. The largest deletion was identified in patient 6 with arr 1q43q44(238 888 870–249 212 668) × 1.
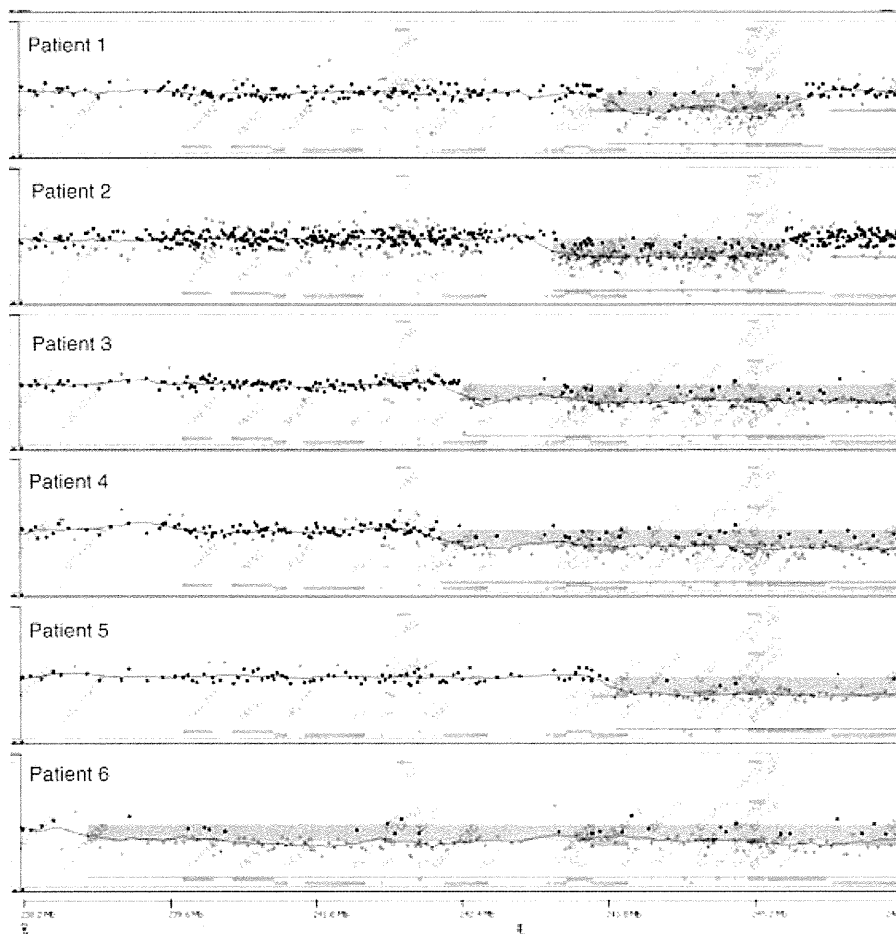

Figure 1 Results of chromosomal microarray testing presented by Gene View of Agilent Genomic Workbench (Agilent Technologies). Vertical axis and horizontal axis represent log$_2$ signal ratio and genomic position, respectively. Aberrant regions are shown by blue rectangles. Dots indicate the genomic positions and the log$_2$ ratio of each probe.
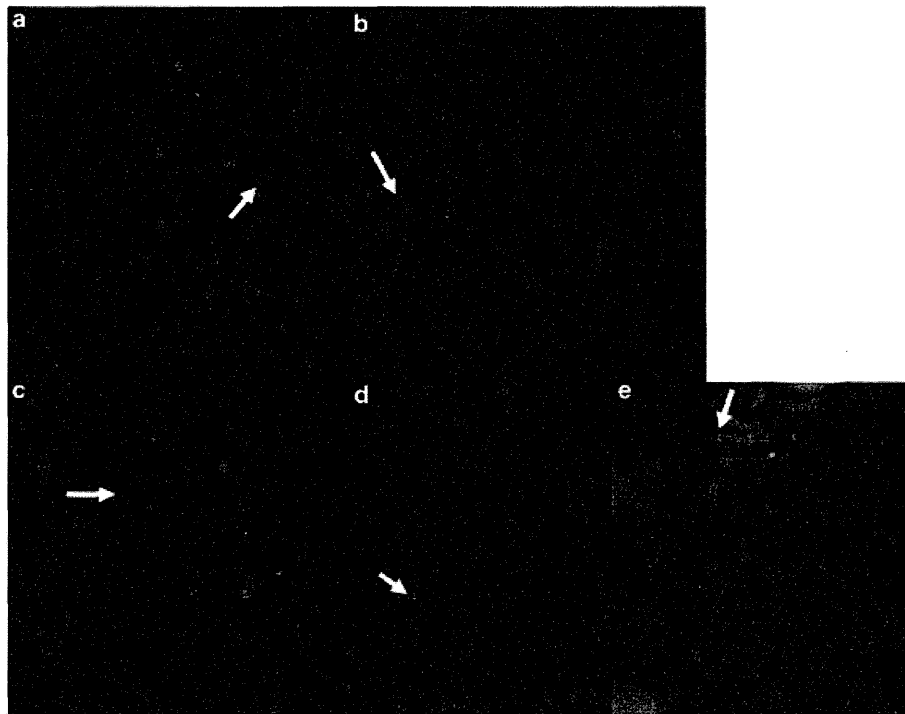
Figure 2 Results of FISH analyses. (a) Loss of the green signal labeling RP11-7L23 (arrow) indicates deletion of 1q44 in patient 1. (b) Loss of the green signal labeling RP11-88N11 (arrow) indicates deletion of 1q44 in patient 3. (c–e) Confirmation of the unbalanced translocation between chromosome 1 and 5 in patient 4. Loss of the green signal labeling RP11-143E8 (arrow) indicates deletion of 1q44 (c). An additional signal labeling RP11-94J21 of 5p15.33 is present on the other chromosome (d, red signal, arrow), indicating a translocation onto chromosome 1 (e, green signal, arrow).

The result of FISH analysis were summarized in Supplementary Table 1.

CLINICAL REPORT
Patient 1
A 9-year-old boy was born by vacuum extraction. His birth weight was 2820 g (within 25th centile), length was 45 cm (= 3rd centile) and occipitofrontal circumference (OFC) was 32.5 cm (10–25th centile). After birth, he displayed feeding problem. His development was mildly delayed with head control attained at 8 months, sitting without support at 15 months, crawling at 24 months and walking alone without support at 44 months. At the age of 11 months, he experienced recurrent febrile seizures. At 18 months of age, he suffered non-febrile seizures. The brain magnetic resonance imaging (MRI) at 4 years of age revealed loss of volume in the frontal lobe, mild abnormal gyral patterns in the frontal lobe and lateral lobe, and ACC (Figures 3a–c). Conventional chromosomal analysis revealed a normal male karyotype.

At present, his height is 119.5 cm (< 3rd centile) and weight is 23.6 kg (10th centile). He exhibits microcephaly with OFC of 47.5 cm (< 3rd centile). He displays distinctive facial features including a flat occipit, coarse face, high nasal bridge, low-set ears and prominent jaw (Figure 4a). He has short tapering fingers and single palmer creases.

Patient 2
A 3-year and 1-month-old girl is a second child of healthy non-consanguineous parents with an unremarkable family history. She was born at 36th week of gestation after an uneventful

pregnancy. She displayed prenatal growth retardation with her weight of 2348 g (< 3rd centile), length of 44.4 cm (< 3rd centile) and OFC of 31 cm (< 3rd centile). At the age of 6 months, developmental delay and microcephaly were noted. She could balance her head at 6 months, sit at 10 months, roll over at 13 months and crawl at 20 months. At the age of 11 months, she suffered febrile convulsion, followed by 11 recurrent attacks of complex febrile seizures. The findings of her electroencephalogram were unremarkable.

At the age of 2 years and 11 months, she had a short stature (height 79 cm, < 3rd centile; weight 10 kg, < 3rd centile) and microcephaly (OFC 42.5 cm, < 3rd centile). Facial dysmorphism included epicanthal folds, a broad nasal root and down-turned corner of mouth (Figure 4b). Neurological examination revealed generalized hypotonia. At this time, she showed moderate psychomotor developmental delay with motor development of 10 months and language development of 8 months. Ultrasonography of the kidneys and liver, echocardiography, ophthalmologic and audiologic examinations revealed no abnormalities. Conventional chromosome analysis revealed a normal female karyotype.

At present, the patient cannot stand without support. She can speak only babbled words. The brain MRI revealed ACC and loss of the volume of the frontal lobe (Figures 3d–f).

Patient 3
A 1-year and 6-month-old girl was born at the gestational age of 38 weeks by vaginal delivery. Although her pregnancy was unremarkable, she showed prenatal growth retardation with her birth weight of 2040 g (< 3rd centile) and OFC of 30 cm (< 3rd centile). Her APGAR score was 9/9. One hour after birth, she suffered a convulsion